Available online at www.sciencedirect.com
ScienceDirect
Journal of Photochemistry and Photobiology A: Chemistry 182 (2006) 335–341
Journal of Photochemistry and Photobiology A:Chemistry
www.elsevier.com/locate/jphotochem

Preparation of metal oxide-based nanomaterials using nanosecond pulsed laser ablation in liquids

Takeshi Sasaki *, Yoshiki Shimizu, Naoto Koshizaki

Nanoarchitectonics Research Center, National Institute of Advanced Industrial Science and Technology (AIST), Central 5, 1-1-1 Higashi, Tsukuba, Ibaraki 305-8565, Japan

Available online 3 July 2006

Abstract

Numerous experiments for nanomaterial fabrication using pulsed laser ablation in liquid have been reported. Most studies have focused on the formation of noble-metal nanoparticles and their surface plasma-resonant optical properties. This short review highlights the fabrication of metal oxide-based nanomaterials such as oxide and hydroxide nanoparticles, as well as layered nanocomposites, via nanosecond pulsed laser ablation of metallic target materials in water and aqueous surfactant solutions. These crystallized oxide-based nanomaterials are formed through the ejection of ablated species with extremely high density and high kinetic energy followed by oxidation in the liquid.

Keywords: Pulsed laser ablation in liquid; Nanoparticles; Nanocomposite; Oxide; Hydroxide

1. Introduction

Pulsed laser ablation in liquid media (PLAL) is a promising technique for the controlled fabrication of nanomaterials via rapid reactive quenching of ablated species at the interface between the plasma and liquid. PLAL is a versatile technique for preparing various kinds of nanoparticles (NPs) such as noble metals [1,2], alloys [3,4], oxides [5–16] and semiconductors [17]. The features of PLAL are as follows. Well crystallized NPs can easily be obtained in one-step procedures without subsequent heat-treatments [8,9] because of the high energetic state of ablated species [18–20]. Certain pure NP colloidal solutions can be formed without the formation of by-products. In addition, chemicals such as surfactants can be added to liquids in order to control the size and the aggregation state of NPs by changing the surface charge of the nuclei [13,21]. The entire product can be completely collected in solutions, and the obtained colloid solution is very easy to handle. The production system does not require costly vacuum chambers.

The fabrication of noble-metal NPs has been studied extensively because of their characteristic optical absorption by surface plasmon resonance. The nanomaterials initially prepared by PLAL were noble-metal NPs [22,23], and controlled formation of noble-metal NPs has been achieved using aqueous surfactant solutions [24]. Femtosecond laser ablation in liquids can also be employed to prepare very small and monodispersed noble-metal particles [25,26]. This technique can also be applied to the fabrication of novel nanomaterials, including metastable and nonequilibrium phases, via rapid reactive quenching of ablated species with extremely high density and high kinetic energy. The formation of nanodiamond [27,28] and cubic-BN [29,30] by PLAL has been reported. Furthermore, organic and inorganic nanocomposites can be formed by the interaction between ablated inorganic species and surfactant molecules in liquids [6,12].

Various metal-oxide NPs have been also prepared by PLAL. The concept of fabricating oxide using laser irradiation of metal targets in water was demonstrated in 1987, where iron and tantalum oxides were formed on target surfaces in water using a Q-switched ruby pulsed laser [31,32]. Although the preparation of various kinds of NPs by ablation of different targets in deionized water has been extensively studied in recent days, papers reporting the fabrication of metal oxide-based nanomaterials from metal targets by PLAL are still scarce compared with reports concerning the production of noble-metal NPs.

This short review aims to summarize recent research on the preparation of metal oxide-based nanomaterials such as oxide NPs and nanocomposites using pulsed laser ablation of metal targets in aqueous solutions. The formation mechanism of the nanomaterials is also discussed.

* Corresponding author. Tel.: +81 29 861 4896; fax: +81 29 861 6355.
E-mail address: takeshi.sasaki@aist.go.jp (T. Sasaki).

1010-6030/$ – see front matter © 2006 Elsevier B.V. All rights reserved.
doi:10.1016/j.jphotochem.2006.05.031

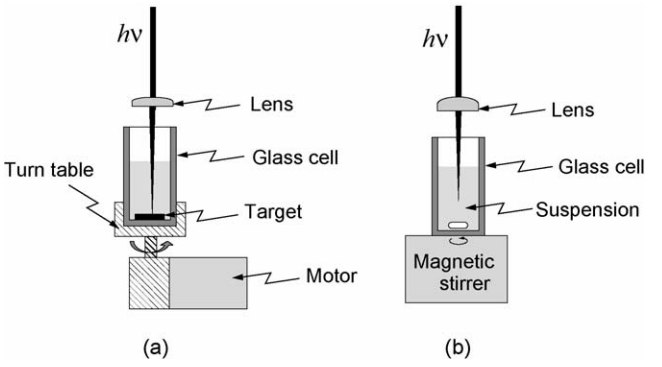

Fig. 1. Typical experimental setup for laser ablation in liquids. The target is rotated during laser irradiation (a). The suspension is also irradiated by the laser, with the focal point in the solution (b), but the spot size on the suspension surface was adjusted in some cases.

2. Experimental procedures of PLAL

Fig. 1 illustrates a typical experimental setup for PLAL [15,33]. A high-purity metallic plate is fixed at the bottom of a glass cell as the target and is rotated to avoid a deep ablation trace, as shown in Fig. 1a, because the deep trace can bring about the change of the spot size. Metallic particles dispersed in liquids can also be irradiated by a pulsed laser as depicted in Fig. 1b. A short overview of the ablation of metals in aqueous solutions is presented in Table 1, where the target, laser conditions, solutions, products, etc. are indicated. Typical pulse energy for PLAL ranges from a few tens to several hundreds millijoules per pulse. The laser beam is focused by a lens with a focal length from 10 to 250 mm in order to get sufficient laser fluence for the ablation. The typical diameter of the laser spot on a bulk target changes from 0.05 to 2.0 mm and the typical liquid volume range is 5–20 ml. Certain chemicals such as surfactants can be added to the solution to control the size and aggregation of the products. A nanosecond Nd:YAG laser is most frequently used as the light source. High-order harmonic waves can also be used for ablation. After laser irradiation ranging from 10 to 120 min, a colloidal solution of oxide-based nanomaterials can be obtained. In the case of open cells depicted in Fig. 1, liquid droplets are sometimes ejected from the solution surface under laser irradiation and deposited on the lens. This phenomenon must be avoided in order to maintain the laser irradiation conditions. A centrifuge and/or super centrifuge is sometimes employed to collect and clean the products. The aging process in the obtained suspension can result in changes in shape of the nanostructures and crystallization in some cases.

A variety of analysis techniques are used for the characterization of products. Morphological observation by transmission-electron microscope (TEM) and scanning-electron microscope

Table 1
Metal oxide-based nanomaterials prepared by ablation of metal targets in aqueous solutions

Target	Laser	Solution	Products	Size	Remarks	Reference
Ti	Nd:YAG 355 nm, 150 mJ/pulse, Ø 1 mm	Water Water + SDS[a]	NP amorphous TiO_2 NP TiO_2 (anatase)	3–150 nm 3 nm		[7,8]
Ti	Cu vapor laser (510.6, 578.2 nm), 20–40 μJ/pulse, Ø 50 μm	Water	NP TiO_x ($x = 1.04$)	35 nm		[37,38]
Sn	Nd:YAG 355 nm, 100 mJ/pulse, Ø 1 mm	Water Water + SDS[a]	NP SnO_2 + Sn NP SnO_2	SnO_2: 2–6 nm Sn: 250 nm		[9]
Zn	Nd:YAG 355 nm, 100 mJ/pulse, Ø 1.5 mm	Water Water + LDA[b] Water + OGM[b] Water + CTAB[b]	NP ZnO	38 nm 12–17 nm 25–25 nm 30–33 nm		[13]
Zn	Nd:YAG 1064 nm, 70 mJ/pulse, Ø 2 mm	Water Water + SDS[a]	NP Zn + ZnO Zn/ZnO core shell	45 nm 37–18 nm		[44]
Al	Nd:YAG 532 nm, 80 mJ/pulse	Water	NP amorphous $Al(OH)_2$, AlOOH	3–300 nm	Re-crystallization occurred by aging	[45,46]
Ga	Nd:YAG 1064 nm, 80 mJ/pulse	Water + CTAB[b]	GaOOH	–	Re-crystallization occurred by aging	[47]
Mg	Nd:YAG 355 nm, 100 mJ/pulse, Ø 1 mm	Water Water + SDS[a]	$Mg(OH)_2$ $Mg(OH)_2$	1–2 nm –	 Tubular and spindle-like structures	[5]
Co	Nd:YAG 355 nm, 30 mJ/pulse	Water	NP Co_3O_4	<10 nm, microparticles (diameter: 20–200 nm) is also included	Powder (diameter: 2 μm) was used as target	[15]
Zn	Nd:YAG 355 nm, 100 mJ/pulse, Ø 1.5–2.25 mm	Water + SAS[a]	Layered nanocomposite with β-$Zn(OH)_2$ and SAS[a]		Carbon number n in SAS[a] = 12, 13, 14 and 16	[6,12,33]

[a] SDS is one of the sodium alkyl sulfates (SAS), $C_nH_{2n+1}SO_4^-{\cdot}Na^+$, with carbon member n of 12.
[b] LDA, OCM, CTAB are lauryl dimethylaminoacetic acid betaine, octaethylene glycol monododecyl ether, and cetyltrimethylammonium bromide.

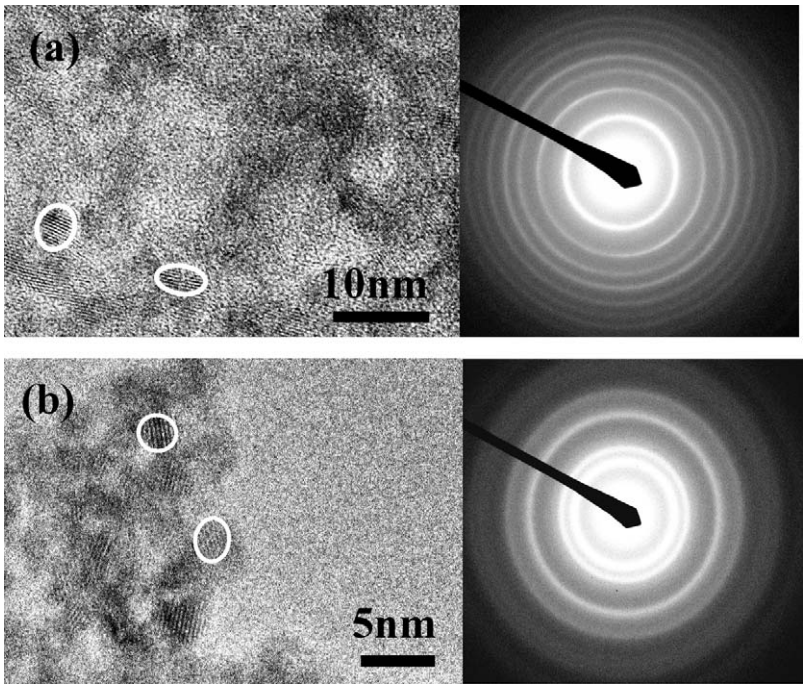

Fig. 2. TEM images and TED patterns of TiO_2 and SnO_2 NPs prepared in a 1×10^{-2} M SDS solution by laser ablation of Ti and Sn targets with the third harmonic of Nd:YAG at 355 nm.

(SEM) is frequently utilized. The optical transmittance and photoluminescence of colloidal solutions are also recorded. X-ray diffraction (XRD) and transmission-electron diffraction (TED) analysis is used for crystallographic structure analysis of the products. Other analytical techniques such as Raman and Fourier transform infrared (FTIR) spectroscopy are also used to characterize the products.

3. Preparation of oxide NPs

3.1. NPs of TiO_2 and SnO_2

Titanium oxide and tin oxide are n-type semiconductors and are very promising materials for photovoltaic cells [34] and gas sensors [35,36]. These nanoparticles have been prepared using wet chemical approaches such as the sol–gel and precipitation methods. In these techniques annealing of the precursors is generally required for their decomposition and for the crystallization of the oxides. In contrast, PLAL provides a very simple, one-step procedure for obtaining crystallized-oxide NPs without any post-process heat-treatments. Laser ablation of Ti in water by a Cu vapor laser (at 510.6 nm with some fraction at 578.2 nm) resulted in the formation of non-stoichiometric oxide of the TiO_x NPs with $x = 1.04$ and an average particle size of 35 nm estimated by X-ray diffraction analysis [37,38]. Much smaller NPs of TiO_2 and SnO_2 were prepared by laser ablation of the corresponding metal targets in an aqueous solution of sodium dodecyl sulfate (SDS; $C_{12}H_{25}SO_4Na$), using the third harmonic of a Nd:YAG laser (355 nm) [7,9]. Fig. 2 presents TEM images and TED patterns of TiO_2 and SnO_2 NPs prepared in a 1×10^{-2} M SDS solution. The NP size ranged from 2 to 6 nm in diameter. As can be seen in the TED patterns in Fig. 2, each pattern shows halo diffraction rings resulting from well crystallized-oxide NPs. The crystal structure of the oxide NPs was identified as anatase TiO_2 (JCPDS 21-1272) and cassiterite SnO_2 (JCPDS 77-448). These results were very consistent with an XRD analysis of the dropcast films of these oxide NPs. It should be noted that the crystallinity of the obtained oxide NPs was strongly affected by the concentration of SDS in the solution. Most well crystallized-oxide NPs were prepared in solutions around the critical micelle concentration (CMC) for SDS (8.6×10^{-3} M).

According to a previous study involving laser ablation at solid–liquid interfaces, a laser-induced plasma may be generated on a target in liquid as well as one in gas. Such a plasma includes quite highly energetic species of atoms, ions and clusters confined in the solution [18–20]. Diagnostics for laser-induced plasma in water have indicated that the temperatures and pressures can instantaneously reach 1×10^4 to 1×10^5 K and a few GPa range [39,40]. These energetic species can react and are quenched when they enter in contact with water molecules, forming nuclei of oxide or hydroxide via instantaneous hydrothermal oxidation. Surfactant molecules in the water could play an important role in the growth, ripening and aggregation of these nuclei. Although the detailed mechanisms of the crystallization of NPs are not yet clear, instantaneous and localized high temperature and high pressure fields at the edge of the ablation shockwave may enhance crystallization. As can be seen in Fig. 1, NPs formed in solution can also be irradiated within the optical path above the spot point on the target by a laser during ablation. Such post-irradiation of the product by laser may also improve the crystallinity of the NPs via laser heating. In this case, the suppression of the coagulation of NPs by surfac-

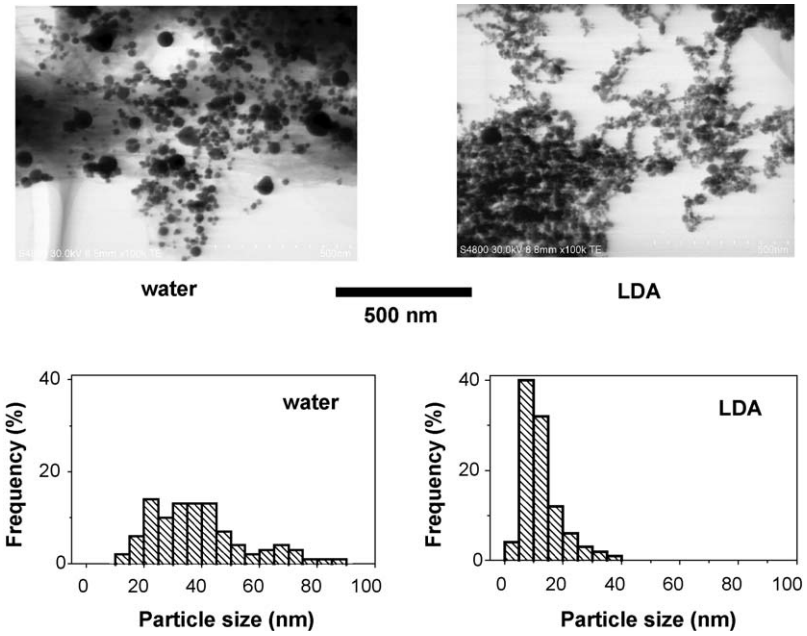

Fig. 3. Scanning transmission electron microscopic images captured by a field emission SEM and histograms of the size of ZnO NPs prepared by laser ablation of zinc plate in deionized water and 1×10^{-2} M LDA with the third harmonic of Nd:YAG at 355 nm.

tants is very important in avoiding scattering of the laser light. Therefore, a maximum amount of stable colloidal suspension of crystallized TiO_2 and SnO_2 NPs can be obtained around the CMC.

3.2. Zinc oxide NPs and their photoluminescence properties

ZnO is an oxide semiconductor of interest for ultraviolet (UV) LED and UV laser applications due to its wide direct band gap of 3.4 eV [41]. In addition, its exciton binding energy of 60 meV exceeds the room-temperature energy of 26 meV [42]. Therefore, ZnO can achieve excitonic UV emission even at room temperature. ZnO NPs have been widely investigated as an emission material because of the enhancement of their optical and electrical properties caused by the quantum confinement effect [43]. However, surface defects and impurity levels are easily generated during the nanoparticle formation process, and lattice defects in ZnO, such as oxygen vacancies, cause recombination centers for green emission and nonradiative relaxation, resulting in the degradation of UV emission. For the application of ZnO NPs as a UV emitter, suppression of green emission, i.e., the reduction of surface defects, is very important.

ZnO NPs can also be prepared by ablation of a zinc plate using the third harmonic of a Nd:YAG laser in water and aqueous solutions of surfactant. The effects of having different surfactant molecules in the solution on particle size and distribution and on the photoluminescence properties of the obtained ZnO NPs have been investigated in detail [13]. Fig. 3 presents scanning transmission electron microscopic images captured by the field emission SEM and histograms of the size of ZnO NPs prepared in deionized water and in an aqueous solution of lauryldimethylaminoacetic acid betaine (LDA; $CH_3(CH_2)_{11}N(CH_3)_2$ CH_2COO) with a concentration

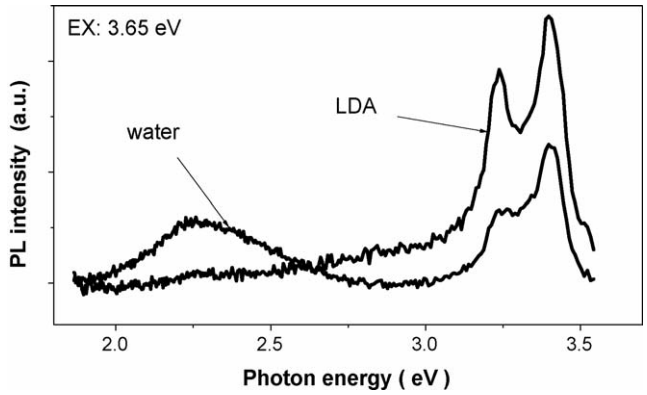

Fig. 4. Photoluminescence emission spectra of the ZnO NP suspension just after ablation, prepared from zinc plate in deionized water and 1×10^{-2} M LDA with the third harmonic of Nd:YAG at 355 nm.

of 1×10^{-2} M. The average size d and standard deviation σ of the ZnO NPs prepared in water were $d = 38$ nm and $\sigma = 16$ nm. These values decreased with increases in the concentration of LDA, reaching $d = 12$ nm and $\sigma = 6.5$ nm at 1×10^{-2} M LDA. Smaller ZnO NPs with a narrower size distribution were generally obtained in the aqueous solution of surfactants with negatively charged molecules due to the effective adsorption caused by charge matching between the positively charged ZnO NPs and the negatively charged molecules. Surfactants adsorbed on the ZnO nuclei and particles during ablation can suppress further growth of the ZnO NPs. In the laser ablation of zinc by the third harmonic of Nd:YAG, however, typical anionic surfactants of sodium alkyl sulfate that have a negative charge in solution resulted in completely different nanomaterial formation, as described in the next section.

Fig. 4 depicts the photoluminescence spectra of the ZnO NP suspension obtained just after ablation in deionized water and 1×10^{-2} M LDA. The aqueous solution of LDA has no luminescence in this wavelength region, and the peaks observed at 3.27 eV are assigned to Raman scattering of the water. A UV exciton and broad defect emission peaks are observed at 3.40 and 2.29 eV. It should be noted that the broad defect emission peak completely disappears and the UV emission intensity is increased in ZnO NPs prepared in the LDA solution. These results indicate that LDA molecules can passivate surface oxygen defects. LDA is an amphoteric surfactant that possesses a localized negative charge on the oxygen in the carboxyl ion and a localized positive charge on the nitrogen. LDA adsorbed on ZnO NP surfaces would effectively passivate any oxygen defects.

Zn/ZnO core shell structures have also been prepared by laser ablation of Zn using the fundamental of Nd:YAG at 1064 nm in an SDS solution [44]. Ablation of zinc by an infrared laser generates spherical zinc NPs with diameter from 20 to 100 nm, which could be originated from molten droplet formed via explosive boiling of the target, and the subsequent oxidation of these particles forms the oxide shell. The SDS molecules can suppress this oxidation by forming a bi-layer micelle. The shell structures were strongly dependent on the concentration of SDS. The Zn/ZnO core shell structures have a blue luminescence in the 440–550 nm range that is attributable to interstitial zinc in the ZnO lattice.

Pulsed laser ablation of a zinc target in water using fundamental and third harmonic Nd:YAG laser could essentially result in formation of metal and oxide NPs. These results are suggestive of the potential control of nanomaterial fabrication by different laser wavelengths, which would arise from the different optical and thermal interactions with target materials.

3.3. NPs of other oxides and hydroxides

NPs of other metal oxides and hydroxides have also been prepared by the ablation of metal in water. Aluminum hydroxides were prepared by laser ablation of an Al rod immersed in water using the second harmonic of a Nd:YAG laser (532 nm) [45,46]. Differently shaped hydroxide particles in the nanometer range were obtained via aging of the prepared suspension after the ablation. The shapes were triangular (bayerite), rectangular (gibbsite) and fibrous (boehmite). The ablated Al species reacts with the water to yield an amorphous gel that transforms to the crystallized aluminum hydroxide by aging. The dissolution and re-crystallization process plays an important role in the development of aluminum hydroxides. Similarly, gallium oxyhydroxide NP formation via the aging process, where gallium metal was ablated by a Nd:YAG laser (1064nm) in a cetyltrimethylammonium bromide (CTAB) surfactant solution has also been reported [47]. Unique nanostructures of magnesium hydroxide have also been prepared by laser ablation of magnesium plate in aqueous solutions of SDS [5]. The obtained nanostructures strongly depended on the concentration of the surfactant. A wormhole-like bulk gel was obtained in deionized water after drying at room temperature. The gel exhibited crystallized pore walls without any post-calcination. Ultrafine tubular fibers were formed in lower concentrations of SDS solution. Stripe-like rods and large platelets grew preferentially with increased surfactant concentration.

NPs of cobalt oxide have been prepared by laser irradiation of Co metal particles in water, using a third harmonic Nd:YAG laser (355 nm). Particles of cobalt oxide such as CoO and Co_3O_4 were also used in these experiments [15]. Co_3O_4 NPs were produced from all target powders in water. When an organic solvent of hexane was used, NPs of cobalt metal were obtained from Co and Co_3O_4 particles. These results indicate that water is very important for the oxidation of ablated species. Ablation of oxide targets in water can form oxide nanoparticles. Differences between oxide and metal targets may not affect the phase of the obtained oxide. The optical and thermal properties of the target materials affect ablation yields, which may change the particle size and the production efficiency of the oxide NPs.

4. Preparation of organic/inorganic nanocomposites

Layered organic/inorganic nanocomposites composed of an inorganic layer and a dodecyl sulfate lamella can be prepared by laser ablation of zinc in an aqueous solution of SDS [6]. SDS is a typical anionic surfactant from the sodium alkyl sulfate group, $C_nH_{2n+1}SO_4^-{\cdot}Na^+$, with an alkyl chain length $n = 12$. Fig. 5

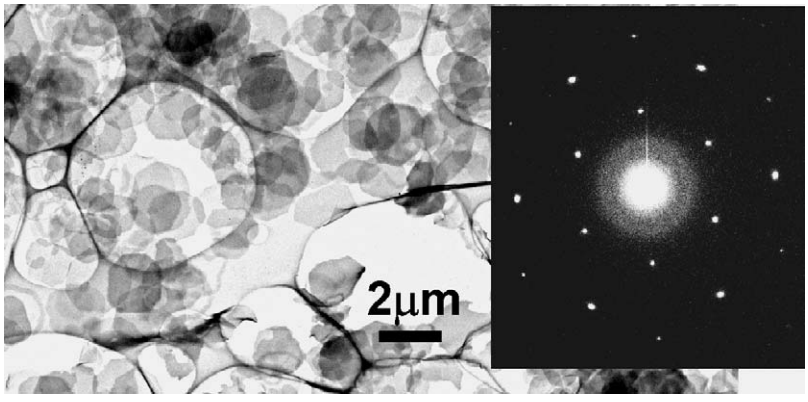

Fig. 5. Typical TEM image and TED pattern of layered organic/inorganic nanocomposites prepared by laser ablation of Zn plate in 1×10^{-2} M SDS with the third harmonic of Nd:YAG at 355 nm.

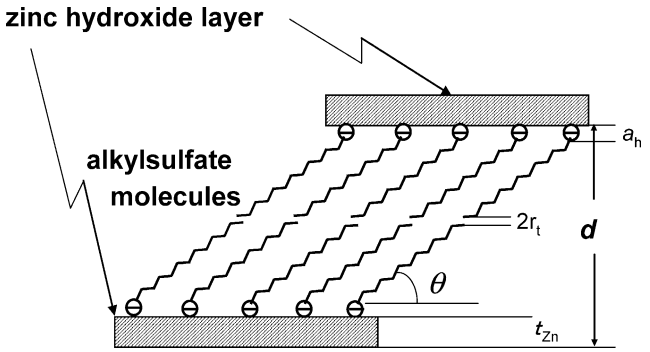

Fig. 6. Structural schematic of a layered organic/inorganic nanocomposite prepared in a sodium alkyl sulfate solution.

presents a typical TEM image and TED pattern for the obtained nanocomposite. The nanocomposites have unique structures, e.g. octagon-shaped platelets and hexagonal in-plane crystallographic symmetry. It was inferred from a detailed chemical analysis that the nanocomposite is a layered single crystal composed of β-$Zn(OH)_2$ layers that intercalate the dodecyl sulfate tilted lamella as illustrated in Fig. 6.

The effect of the alkyl chain length n of the surfactants on the structures of the obtained nanocomposite has also been examined [12,33]. A layered organic/inorganic nanocomposite was obtained only with specific sodium alkyl sulfates ($n = 12$, 13, 14 and 16). The structure of the layered organic/inorganic nanocomposite depicted in Fig. 6 is characterized by two parameters: the inorganic layer-to-layer spacing, d, and the tilting angle of the alkyl chain, θ. The value for d was calculated from XRD diffraction data for the layered nanocomposites, and θ was estimated using the following equation:

$$d = t_{Zn} + 2r_t + 2a_h + 2 \times 1.27n \sin\theta, \quad (1)$$

where t_{Zn} is the minimum thickness of the inorganic layer (7.3 Å), r_t is the end tail size of an alkyl chain (1.5 Å), a_h is the size of the head group in an alkyl sulfate (1.97 Å) and n is the carbon number of the alkyl sulfate. In Eq. (1), $1.27n$ corresponds to the length of an alkyl chain in the surfactant molecule. The structural characteristic parameters of d and θ increased with increasing carbon number n from 26.8 to 42.0 Å and from 27.3° to 43.1°, respectively. Thus, the structure of a layered organic/inorganic nanocomposite can easily be controlled by varying the alkyl sulfate chain length.

The obtained organic/inorganic nanocomposites have an inorganic layer of β-$Zn(OH)_2$, which is the high temperature and pressure phase of zinc hydroxide [6]. In the nanocomposite, these hydroxide layers have the defects of the hydroxyl group, giving rise to a positive charge in the layers that can combine with the negatively charged dodecyl sulfate ions. The formation mechanism of the nanocomposite is as follows. First, zinc hydroxide nuclei with OH defects are formed by laser ablation of zinc. These positively charged nuclei merge with negatively charged dodecyl sulfate ions to form the nanocomposite by self-assembly with charge matching. The formation of the high temperature and pressure phase of zinc hydroxide suggests the existence of a hydrothermal reaction in water resulting from the instantaneous high temperature and pressure field generated by laser ablation.

5. Concluding remarks

Pulsed laser ablation in liquid is a remarkable, unique process for the fabrication of nanomaterials using the physical laser ablation phenomenon and subsequent chemical reactions. Metal oxide-based nanomaterials such as oxide and hydroxide NPs, as well as layered nanocomposites that are very difficult to prepare by only a chemical reaction, can easily be prepared from metallic targets through simple one-step procedures. These oxide-based nanomaterials are formed via aqueous oxidation of ablated species ejected from the metallic target in water by laser ablation. However, the detailed mechanisms are not completely clarified compared with laser ablation in a vacuum or ambient gas because the breakdown of the liquid in the process must also be taken into account. Further detailed investigation using both experimental and theoretical techniques is required to develop this method into a useful nanomaterials production regime.

Acknowledgement

This work was partially supported by the Industrial Technology Research Grant Program 2005 from the New Energy and Industrial Technology Development Organization (NEDO) of Japan.

References

[1] T. Tsuji, N. Watanabe, M. Tsuji, Appl. Surf. Sci. 211 (2003) 189.
[2] F. Mafune, J.Y. Kohno, Y. Takeda, T. Kondow, J. Phys. Chem. B 107 (2003) 4218.
[3] S.H. Tsai, Y.H. Liu, P.L. Wu, C.S. Yeh, J. Mater. Chem. 13 (2003) 978.
[4] J. Zhang, J. Worley, S. Denommee, C. Kingston, Z.J. Jakubek, Y. Deslandes, M. Post, B. Simard, N. Braidy, G.A. Botton, J. Phys. Chem. B 107 (2003) 6920.
[5] C.H. Liang, T. Sasaki, Y. Shimizu, N. Koshizaki, Chem. Phys. Lett. 389 (2004) 58.
[6] C.H. Liang, Y. Shimizu, M. Masuda, T. Sasaki, N. Koshizaki, Chem. Mater. 16 (2004) 963.
[7] C.H. Liang, Y. Shimizu, T. Sasaki, N. Koshizaki, Appl. Phys. A 80 (2005) 819.
[8] C.H. Liang, Y. Shimizu, T. Sasaki, N. Koshizaki, J. Mater. Res. 19 (2004) 1551.
[9] C.H. Liang, Y. Shimizu, T. Sasaki, N. Koshizaki, J. Phys. Chem. B 107 (2003) 9220.
[10] T. Sasaki, C. Liang, W.T. Nichols, Y. Shimizu, N. Koshizaki, Appl. Phys. A 79 (2004) 1489.
[11] H. Usui, T. Sasaki, N. Koshizaki, Appl. Phys. Lett. 87 (2005).
[12] H. Usui, T. Sasaki, N. Koshizaki, Chem. Lett. 34 (2005) 700.
[13] H. Usui, Y. Shimizu, T. Sasaki, N. Koshizaki, J. Phys. Chem. B 109 (2005) 120.
[14] T. Tsuji, T. Kakita, T. Hamagami, T. Kawamura, J. Yamaki, M. Tsuji, Chem. Lett. 33 (2004) 1136.
[15] T. Tsuji, T. Hamagami, T. Kawamura, J. Yamaki, M. Tsuji, Appl. Surf. Sci. 243 (2005) 214.
[16] A. Iwabuchi, C.K. Choo, K. Tanaka, J. Phys. Chem. B 108 (2004) 10863.
[17] K.V. Anikin, N.N. Melnik, A.V. Simakin, G.A. Shafeev, V.V. Voronov, A.G. Vitukhnovsky, Chem. Phys. Lett. 366 (2002) 357.

[18] K. Saito, T. Sakka, Y.H. Ogata, J. Appl. Phys. 94 (2003) 5530.
[19] T. Sakka, S. Iwanaga, Y.H. Ogata, A. Matsunawa, T. Takemoto, J. Chem. Phys. 112 (2000) 8645.
[20] T. Sakka, K. Saito, Y.H. Ogata, J. Appl. Phys. 97 (2005).
[21] J.P. Sylvestre, A.V. Kabashin, E. Sacher, M. Meunier, J.H.T. Luong, J. Am. Chem. Soc. 126 (2004) 7176.
[22] A. Fojtik, A. Henglein, Ber. Bunsen-Ges. Phys. Chem. Chem. Phys. 97 (1993) 252.
[23] J. Neddersen, G. Chumanov, T.M. Cotton, Appl. Spectrosc. 47 (1993) 1959.
[24] F. Mafune, J. Kohno, Y. Takeda, T. Kondow, H. Sawabe, J. Phys. Chem. B 105 (2001) 5114.
[25] A.V. Kabashin, M. Meunier, J. Appl. Phys. 94 (2003) 7941.
[26] T. Tsuji, T. Kakita, M. Tsuji, Appl. Surf. Sci. 206 (2003) 314.
[27] C.X. Wang, Y.H. Yang, G.W. Yang, J. Appl. Phys. 97 (2005).
[28] C.X. Wang, Y.H. Yang, Q.X. Liu, G.W. Yang, Y.L. Mao, X.H. Yan, Appl. Phys. Lett. 84 (2004) 1471.
[29] J.B. Wang, G.W. Yang, C.Y. Zhang, X.L. Zhong, Z.H.A. Ren, Chem. Phys. Lett. 367 (2003) 10.
[30] Q.X. Liu, G.W. Yang, J.X. Zhang, Chem. Phys. Lett. 373 (2003) 57.
[31] S.V. Ghaisas, A.P. Malshe, P.P. Patil, S.M. Kanetkar, S.B. Ogale, V.G. Bhide, J. Appl. Phys. 62 (1987) 2799.
[32] P.P. Patil, D.M. Phase, S.A. Kulkarni, S.V. Ghaisas, S.K. Kulkarni, S.M. Kanetkar, S.B. Ogale, V.G. Bhide, Phys. Rev. Lett. 58 (1987) 238.
[33] T. Sasaki, C.H. Liang, H. Usui, Y. Shimizu, N. Koshizaki, Proc. Mater. Res. Soc. 847 (2005) 243.
[34] P.V. Kamat, in: J.H. Fendler (Ed.), Nanoparticles and Nanostructures Films, Wiley-VCH, New York, 1998, p. 207.
[35] G. Williams, G.S.V. Coles, J. Mater. Chem. 8 (1998) 1657.
[36] G. Williams, G.S.V. Coles, MRS Bull. 24 (1999) 25.
[37] S.I. Dolgaev, A.V. Simakin, V.V. Voronov, G.A. Shafeev, F. Bozon-Verduraz, Appl. Surf. Sci. 186 (2002) 546.
[38] A.V. Simakin, V.V. Voronov, N.A. Kirichenko, G.A. Shafeev, Appl. Phys. A 79 (2004) 1127.
[39] L. Berthe, R. Fabbro, P. Peyre, E. Bartnicki, J. Appl. Phys. 85 (1999) 7552.
[40] L. Berthe, R. Fabbro, P. Peyre, L. Tollier, E. Bartnicki, J. Appl. Phys. 82 (1997) 2826.
[41] I. Ozerov, M. Arab, V.I. Safarov, W. Marine, S. Giorgio, M. Sentis, L. Nanai, Appl. Surf. Sci. 226 (2004) 242.
[42] M. Kawasaki, A. Ohtomo, I. Ohkubo, H. Koinuma, Z.K. Tang, P. Yu, G.K.L. Wong, B.P. Zhang, Y. Segawa, Mater. Sci. Eng. B-Solid State Mater. Adv. Technol. 56 (1998) 239.
[43] Y. Wang, N. Herron, J. Phys. Chem. 95 (1991) 525.
[44] H.B. Zeng, W.P. Cai, Y. Li, J.L. Hu, P.S. Liu, J. Phys. Chem. B 109 (2005) 18260.
[45] H.M. Kao, R.R. Wu, T.Y. Chen, Y.H. Chen, C.S. Yeh, J. Mater. Chem. 10 (2000) 2802.
[46] Y.P. Lee, Y.H. Liu, C.S. Yeh, PCCP Phys. Chem. Chem. Phys. 1 (1999) 4681.
[47] C.C. Huang, C.S. Yeh, C.J. Ho, J. Phys. Chem. B 108 (2004) 4940.